A Real-Time Signal Quality Monitor For GPS Augmentation Systems

Alexander M. Mitelman, R. Eric Phelts, Dennis M. Akos,
Samuel P. Pullen, Per K. Enge

Stanford University

BIOGRAPHY

Alexander Mitelman is a Ph.D. candidate in the Department of Electrical Engineering at Stanford University. As a member of the GPS Laboratory, his research is focused on local area differential GPS design, signal analysis, and applications. Mr. Mitelman received his S.B. in Electrical Engineering from the Massachusetts Institute of Technology in 1993 and his M.S. in Electrical Engineering from Stanford University in 1995.

R. Eric Phelts is a Ph.D. candidate in the Department of Aeronautics and Astronautics at Stanford University. He received his B.S. in Mechanical Engineering from Georgia Institute of Technology in 1995, and his M.S. in Mechanical Engineering from Stanford University in 1997. His research involves multipath mitigation and satellite signal anomalies.

Dr. Dennis M. Akos completed the Ph.D. degree in Electrical Engineering at Ohio University within the Avionics Engineering Center. He has since served as a faculty member with Luleå Technical University, Sweden, and is currently a Research Associate with the GPS Laboratory at Stanford University.

Dr. Sam Pullen received his Ph.D. in Aeronautics and Astronautics from Stanford University in 1996. Since graduating, Dr. Pullen has served as Research Associate and as Technical Manager at Stanford, where he has supported GPS Local Area Augmentation System (LAAS) and Wide Area Augmentation System (WAAS) research and development and is now the LAAS project leader. His work in these fields and his support of the Johns Hopkins University Applied Physics Laboratory (JHU/APL) GPS Risk Assessment earned him the ION Early Achievement Award in 1999.

Dr. Per Enge is an Associate Professor in the Department of Aeronautics and Astronautics at Stanford University. He received his B.S. in Electrical Engineering from the University of Massachusetts at Amherst in 1975, and his M.S. and Ph.D., both in Electrical Engineering, from the University of Illinois at Urbana-Champaign in 1979 and 1983. Professor Enge's research focuses on the design of navigation systems which satisfy stringent requirements with respect to accuracy, integrity (truthfulness), time availability, and continuity.

ABSTRACT

The Local Area Augmentation System (LAAS) and the Wide Area Augmentation System (WAAS) are ground-based applications of differential GPS to support aircraft terminal navigation and precision approach. Due to the safety-critical nature of LAAS and WAAS operations and the resulting stringent integrity requirements on system performance, LAAS and WAAS ground facilities must be able to detect any hazardous signal anomalies within a prescribed time-to-alarm (3 seconds for LAAS Category I precision approach). One class of signal-in-space failures that is difficult to detect without specialized monitoring is deformations of the C/A code signals broadcast by GPS satellites. Since code correlator spacings and RF front-end bandwidths may vary between ground and airborne GPS receivers, these deformations, otherwise known as "evil waveforms," may produce hazardous differential ranging errors at the aircraft unless the affected satellites are promptly detected and excluded from the broadcast set of differential corrections.

This paper describes the construction and testing of a prototype real-time signal quality monitor (RTSQM) described in [1]. The first section describes the implementation of the prototype on a personal computer with multiple serial inputs reading data from customized GPS receivers. The discussion covers several design issues of particular interest,

including system timing, simultaneous processing of multiple data streams, and analysis algorithms (including delta and ratio tests using the in-phase values of multiple correlators assigned to each satellite). This system is designed to be integrated into the Stanford LAAS ground system prototype, known as the Integrity Monitor Testbed (IMT).

The second section describes testing of the real-time monitor under both nominal and anomalous signal conditions and present results. The overall test setup uses an arbitrary waveform generator (AWG) and RF circuitry to drive two customized receivers. After collecting nominal data to establish realistic thresholds for SQM test metrics, the threat space of a specific failure mode, the second order step anomaly described in the LAAS Ground Facility Specification [2], is explored in detail.

INTRODUCTION

The Global Positioning System offers a robust source of three-dimensional position information. Thanks to its versatility, GPS is finding increasingly widespread use in civil applications. One class of applications currently under active research is Ground-Based Augmentation Systems (GBAS), in which a ground reference station provides differential corrections to mobile users for precise navigation. In aviation applications, GBAS may also be used for precision approach and landing. A detailed description of one such architecture, the Local Area Augmentation System (LAAS), is presented in [3].

As with any other variant of GPS used in safety-of-life applications, the LAAS must meet strict specifications on integrity, availability and continuity if it is to be used for landing aircraft. In some cases, these specifications lead to conflicting requirements, and meeting all of them simultaneously is a major challenge facing system designers today. In particular, the LAAS must be able to correctly detect and flag any condition which would cause hazardously misleading information (HMI) to be broadcast to airborne users within 3 seconds (the specified LAAS Ground Facility time-to-alarm). On the other hand, the system must not be so conservative as to signal alarms in response to minor, non-hazardous interruptions, as this would lead to unacceptably low system continuity. These requirements are the primary motivation for the design of the RTSQM.

REAL-TIME MONITOR HARDWARE

This section describes the hardware used to perform real-time monitoring. Because a long-term goal for this system is seamless integration into the IMT, the design objective was an easily scalable system (especially to include additional receivers) whose detailed operation was simple to control and modify, if necessary. The hardware setup consists of two basic components: a GPS receiver capable of providing raw data for monitoring and a computer to log the data and process it in real time.

Customized GPS Receiver

Accurate monitoring of the GPS signal being tracked by a receiver requires a more detailed picture of the signal than is typically available. Ordinarily, a receiver's raw correlator outputs are treated as an intermediate result in the process of computing pseudoranges and as such are unavailable to the end user. Additionally, a typical receiver uses a single correlator pair to track a particular signal, so the shape of the underlying correlation peak is not directly observable.

For this research, we used a specially modified NovAtel MiLLennium receiver whose 48 correlators were all assigned to a single channel. The receiver uses a conventional narrow correlator pair (0.1-chip spacing) for signal tracking; the additional correlators are slaved to the code phase estimate provided by the tracking pair. Because this receiver is capable of tracking only one satellite at a time, it cannot calculate a position fix. On the other hand, the receiver locates and tracks an existing signal normally once initialized with that signal's PRN code, and it produces precisely the detailed picture of the correlation peak necessary for signal monitoring and analysis. A picture of the nominal receiver output is shown in Figure 1. The 48-correlator

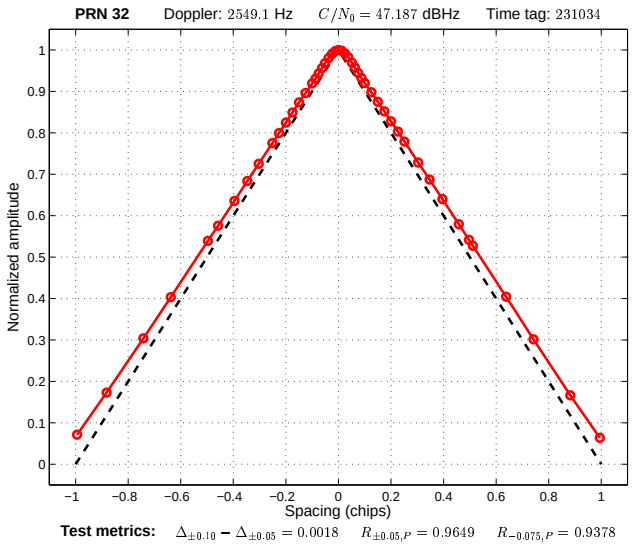

Figure 1: Single-channel 48 correlator receiver

receiver produces raw correlator outputs at 1 Hz, as well as estimates of carrier-to-noise ratio, Doppler shift, and time tag information.

A second customized receiver was also included in the experimental setup. This receiver is similar to the one described above, except that its 48 correlators are evenly distributed across six channels. While this allocation provides a less detailed picture of the correlation peak on a given channel, it is still sufficient to calculate any of the proposed SQM test metrics discussed below. This receiver can compute a position fix and conduct a sky search for new satellites like any conventional receiver. As such, it is appropriate for incorporation into an operational RTSQM; the single-channel receiver, on the other hand, is primarily useful for algorithm development and testing. The single-channel receiver was used for collecting the experimental data presented in this paper.

The data from both receivers is saved to a log file and processed in real time by a standard personal computer, as described in the next section.

Data Processing Platform

The receiver outputs are fed to a test platform consisting of a 550 MHz Pentium III personal computer with 256 MB of memory running the GNU/Linux operating system. Simultaneous data collection from the two receivers is done using a GTek Cyclone six-port serial card and the standard serial port drivers contained in the Linux kernel. A simple C program provides communication, handles all commands sent to the receivers on the multi-port card, and logs all data coming from the receivers to ASCII files. All data processing is done in Matlab.

The real-time operation of the system was verified by logging live satellite data from both receivers simultaneously over the course of several months. The communication between the receivers and the parsing routines worked as expected, generating ASCII log files of approximately 36 MB during 7-hour data collection runs. Correct operation was also observed across end-of-week time tag rollovers.

TEST METRICS

In this section, we describe the operations performed on the incoming raw correlator data.

Prior to processing, smoothed data is obtained from the raw correlator outputs described in the previous section by using a Hatch filter with $N = 100$ for data collected at 1 Hz:

$$I_{\mathrm{smooth}}[k] = \frac{1}{N} I_{\mathrm{raw}}[k] + \frac{N-1}{N} I_{\mathrm{smooth}}[k-1]$$

The resulting smoothed data is combined into a set of algebraic expressions whose values will be compared to known thresholds during monitoring. In the remainder of this paper, we will examine nominal and anomalous signal performance using the delta test metric, defined as

$$\Delta_{\pm\mathrm{offset1},\,\pm\mathrm{offset2}} = \Delta_{\pm\mathrm{offset1}} - \Delta_{\pm\mathrm{offset2}} = \frac{(I_{-\mathrm{offset1}} - I_{+\mathrm{offset1}})}{2 \cdot I_{\mathrm{prompt}}} - \frac{(I_{-\mathrm{offset2}} - I_{+\mathrm{offset2}})}{2 \cdot I_{\mathrm{prompt}}}$$

and three ratio test metrics, defined as

$$R_{\pm\mathrm{offset,P}} = \frac{(I_{-\mathrm{offset}} + I_{+\mathrm{offset}})}{2 \cdot I_{\mathrm{prompt}}}$$

$$R_{+\mathrm{offset,P}} = \frac{I_{+\mathrm{offset}}}{I_{\mathrm{prompt}}}$$

$$R_{-\mathrm{offset,P}} = \frac{I_{-\mathrm{offset}}}{I_{\mathrm{prompt}}}$$

The rationale for using these quantities (instead of the more conventional comparisons of code phase from individual correlator pairs) is discussed in [4]. The expected thresholds for these metrics, using correlator spacings corresponding to SQM variant 2b ($d = 0.1, 0.15, 0.2$ chips), are computed from empirically collected live data in [5]. In all, eleven test metrics were considered (delta tests for two pairs of spacings and three ratio tests – average, positive, and negative, as described above – for each of the spacings individually).

In order to verify the expected thresholds with the real-time monitor setup, live data was collected for a full pass of PRN 20. The elevation angle and three of the test metrics are shown in Figure 2. Each metric stays well within the ex-

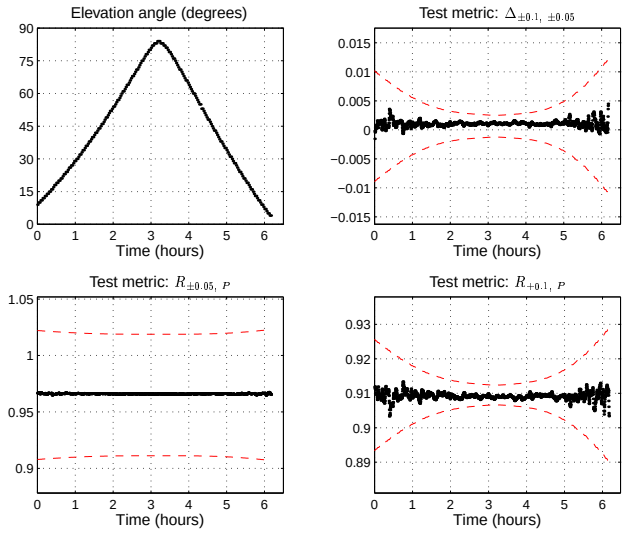

Figure 2: Three test metrics for a full pass of PRN 20

pected thresholds (indicated by the dashed lines) throughout the duration of the run, as expected for nominal data. The "flaring" at the beginning and end of the data set is most likely due to multipath, which is known to cause larger errors at low elevation angles. The nearly noiseless data

shown in the $R_{\pm 0.05,P}$ plot may be explained by observing that this is the tracking pair for this receiver, so we would expect the early and late correlator samples to be balanced at all times (within the noise of the tracking loop).

FAULT MODEL

We next turn our attention to possible signal faults and their effects on the proposed test metrics. To date, a number of satellite-based anomalies have been reported in the literature. A corrupted C/A code spectrum was observed on a healthy satellite in [6]. A transient code outage (later found to be associated with software uploads for Block II satellites) was reported in [7]. A clock event which caused L_1 carrier and C/A code range rates to exceed the Selective Availability NTE specifications for velocity and acceleration was reported in [8].

In this paper, we consider a specific class of digital, analog and mixed-mode signal failures known as the second order step anomaly, as described in [2]. The threat space for this anomaly is defined by three key parameters:

Δ, the amount of lead or lag in the falling edges of the distorted C/A code with respect to the nominal position of those edges;

f_{d}, the ringing frequency associated with the edges of the distorted C/A code; and

σ, the damping coefficient associated with that ringing.

A snapshot of the complete failure mode, including both the digital-domain failure described by Δ and the analog-domain failure described by f_{d} and σ, is shown in Figure 3 (the dashed line is the nominal C/A code). The resulting correlation peak is shown in Figure 4. It is worth noting that the distortions described by f_{d} and σ may be modeled as a simple two-pole linear network for analytical purposes. The lead/lag distortion described by Δ, on the other hand, cannot be easily modeled by a linear system.

In the next section, we consider the problem of generating corrupted signals of the type described above and evaluating their effects on pseudorange errors.

ARBITRARY GPS SIGNAL GENERATION

Because it is impractical to rely on an actual satellite failure to test the real-time monitor, it is necessary to generate test signals locally. This is accomplished by combining a standard RF signal source with a programmable arbitrary waveform generator (AWG), which generates a sampled version of the C/A code.

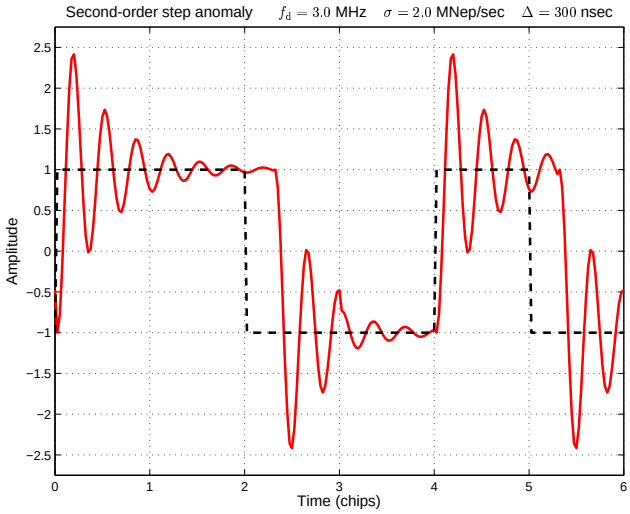

Figure 3: Theoretical effect of second-order step anomaly on C/A code waveform (digital and analog failures)

For this experiment, the code was sampled at 40 points per chip ($f_{\mathrm{s}} = 40.92$ MHz). The output of the AWG was modulated up to the GPS carrier frequency at $L_1 = 1575.42$ MHz, filtered, and attenuated to an appropriate power level. This signal was fed into the antenna input of the 48-correlator receiver described previously. A block diagram of the overall signal generation setup is shown in Figure 5.

Several features are worth noting. First, the entire generator is tied to a common clock. The 10 MHz synchronization signal aligns the carrier zero crossings and the C/A code chip edges, as required for reliable signal tracking.

Another important consideration is signal power. The levels necessary to ensure clean RF mixer operation result in a modulated signal at approximately 0 dBm, which easily saturates the RF front end of the receiver. This signal must be dropped by roughly 125 dB to approximate the level of a real GPS satellite. In our setup, the attenuation chain consists of 110 dB of fixed attenuation and a variable $0-30$ dB pad to model equivalent C/N_0 values from $30-52$ dBHz. This represents the full range observed at all possible elevation angles.

A final consideration is signal parity. In order to be trackable, the locally generated signal must contain enough valid navigation data bits to pass the receiver parity check, as described in [9]. This is done by first creating two 20-epoch strings of C/A code, one with each polarity, representing individual bits of navigation data. A sequence of 30 carefully chosen data bits (600 epochs of C/A code in all) is then programmed into the AWG, resulting in a signal that passes the parity check as required.

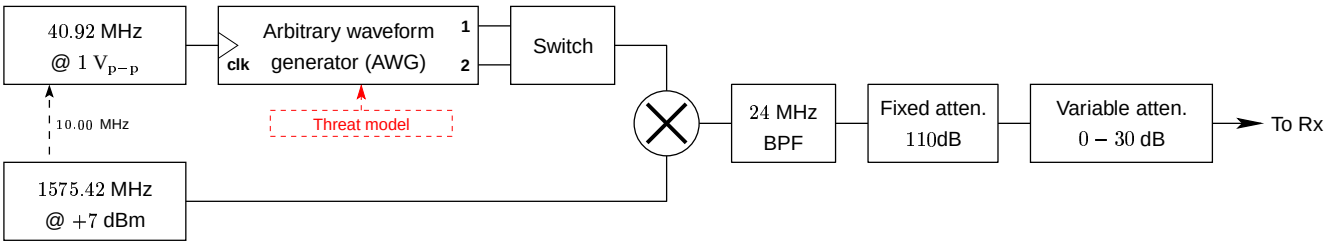

Figure 5: Block diagram of arbitrary GPS signal generator

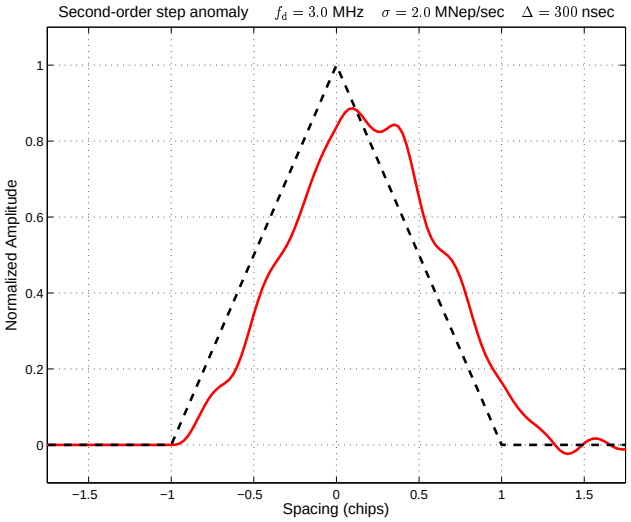

Figure 4: Theoretical effect of second-order step anomaly on correlation peak (digital and analog failures)

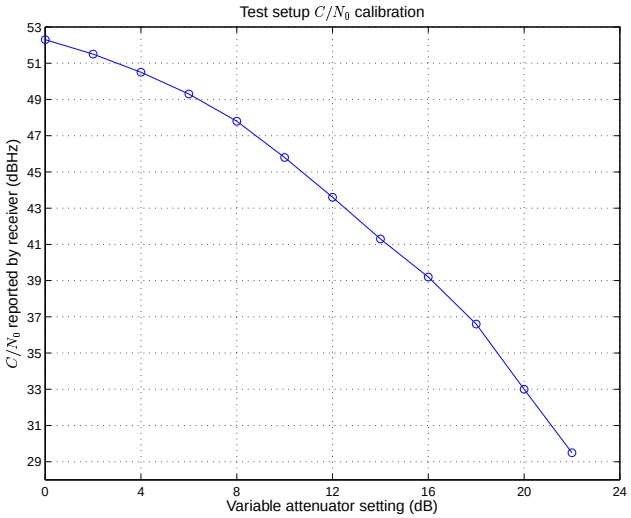

Figure 6: Calibration of variable attenuator settings

Calibration with nominal data

Once a trackable signal is generated, the next step is to calibrate the settings on the variable attenuator to C/N_0 levels reported by the receiver. Nominal C/A code data was fed to the receiver at each attenuator setting and three C/N_0 readings were recorded approximately 30 seconds apart. The average calibration readings, shown in Figure 6, are reasonably linear across the useful range of attenuator settings (the receiver loses lock at an attenuation setting of 23dB).

From the calibration data, three attenuator settings ($8, 14,$ and 20 dB) were chosen to represent high, mid, and low elevation satellites (with C/N_0 of approximately $48, 41,$ and 33 dBHz, respectively). Six hours of nominal data were logged at each setting to verify that the C/N_0 values reported by the receiver were stationary over time. The results are shown in Figure 7. The C/N_0 values reported by the receiver throughout all three runs remained quite stable and agreed reasonably well with the calibration data shown above.

REAL-TIME FAILURE DETECTION

The final part of this experiment investigates the real-time simulation of transient signal failures, that is, the dynamic response of the (smoothed) test metrics to instantaneous onsets of signal anomalies.

Three fault cases were considered for the second-order step anomaly. The parameters are shown in Table 1. A real correlation peak (distorted by fault case 3) is shown in Figure 8. Note that the distorted peak is virtually indistinguishable from the nominal peak near the very top – this suggests that any test metrics involving correlator spacings narrower than about 0.1 chips may not be able to detect this anomaly.

Fault case	f_d (MHz)	σ (MNep/sec)	Δ (nsec)
1	10.0	6.0	30
3	7.6	0.8	0
5	10.0	0.8	90

Table 1: Second-order step fault case parameters

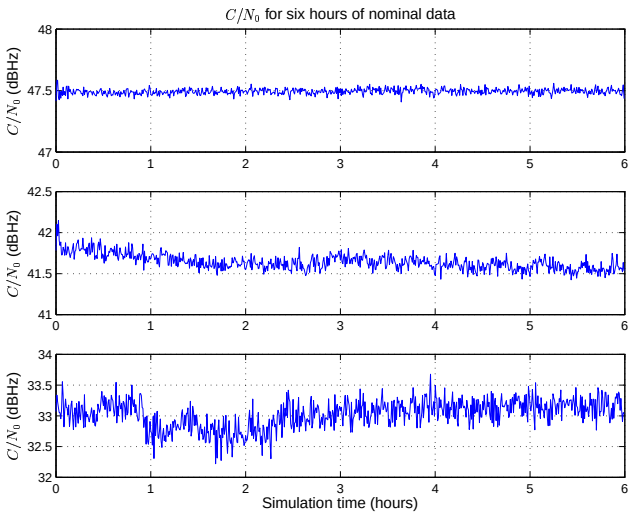

Figure 7: C/N_0 for nominal signals at three attenuator settings: **(a)** 8 dB **(b)** 14dB **(c)** 20dB

Three six-hour data sets (representing high, mid, and low elevation satellites) were collected for fault case 1 and mean (expected) values were computed for the eleven test metrics over each run. Data sets were also collected for fault cases 3 and 5 for high elevation satellites. The expected values of the test metrics for all five runs, as well as for the nominal cases described in the previous section, are summarized in Table 2.

In order to simulate real-time signal failures, the receiver was first supplied with a nominal signal and tracking was maintained for approximately half an hour. The signal was then switched to a second order step waveform of the same (underlying) amplitude and all resulting changes in the test metrics were recorded.

Initially, the signal was switched directly on the front panel of the AWG. It was observed, however, that the slight switching delay (approximately 0.5 sec) consistently caused the receiver to lose signal lock, resulting in large discontinuities in the test metrics. Instead, the two signals were programmed into separate channels of the AWG and a simple SPDT switch was used to simulate the onset of the signal failure. This approach resulted in an instantaneous response on the display with no loss of lock.

One-hour data runs were recorded for fault case 1 at high, mid, and low values of C/N_0. Additionally, two runs were recorded for fault cases 3 and 5, both at high C/N_0. Four representative test metrics are shown for each of the fault cases in Figures 9-11. In each plot, the nominal-to-anomalous transition is indicated by the blue line and the place where each test metric crosses the detection threshold is shown by the green line. The thresholds, in red, are for a high elevation satellite (elevation $= 75°$),

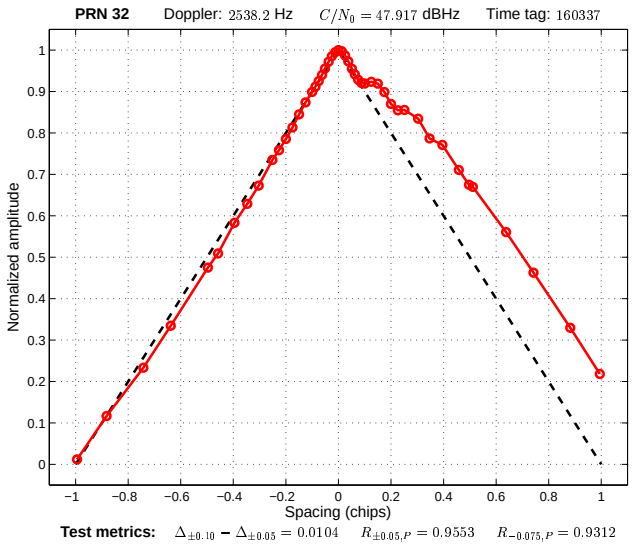

Figure 8: Correlation peak resulting from second-order step anomaly fault case 3

as described in [5].

ANALYSIS OF RESULTS

The dynamic simulations show that the proposed test metrics are all reasonably effective at detecting the sudden onset of second order step anomalies, although the optimal metric depends on the fault case. Both the positive ratio and Δ tests are good choices for detecting fault case 1; the negative ratio test seems best suited for fault case 3; and all but the $R_{-0.05,\ P}$ test detect fault case 5 within 10 seconds.

On the other hand, the three runs of fault case 1 at varying equivalent elevation angle detection thresholds suggest that the negative ratio test would be optimal for this fault case on low elevation angle satellites. The Δ test did not detect the fault at all.

Surprisingly, several test metrics that use correlator samples with spacings less than 0.1 chip wide correctly detect the fault case 3 anomaly discussed earlier. All three ratio tests at 0.05 chip detect the anomaly within 22 seconds. The $\Delta_{\pm 0.1,\ \pm 0.05}$ test also detects the anomaly within this time. By comparison, the $\Delta_{\pm 0.1,\ \pm 0.05}$ test is significantly slower, requiring 65 seconds to exceed the detection threshold. The $R_{\pm 0.1}$ test is even worse, taking 253 seconds.

Table 3 summarizes the detection times for the three different fault cases assuming high elevation detection thresholds. Table 4 summarizes the detection times for fault case 1 for high, medium, and low elevation detection thresholds.

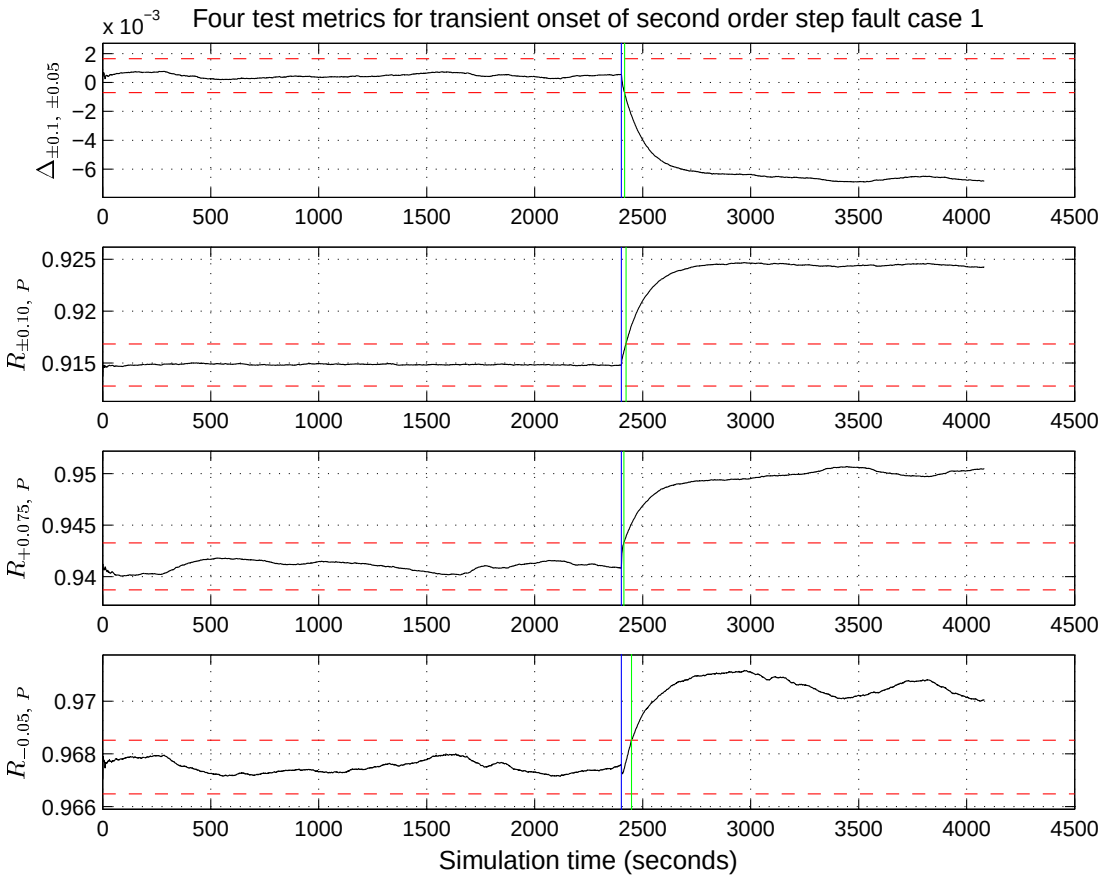

Figure 9: Test metrics for fault case 1

Test metric	FC 1 High	FC 3 High	FC 5 High
$\Delta_{\pm 0.075,\ \pm 0.05}$	9	65	2
$\Delta_{\pm 0.1,\ \pm 0.05}$	15	18	3
$R_{\pm 0.05,\ P}$	33	19	4
$R_{\pm 0.075,\ P}$	28	25	8
$R_{\pm 0.1,\ P}$	22	253	6
$R_{-0.05,\ P}$	47	15	13
$R_{-0.075,\ P}$	61	14	2
$R_{-0.1,\ P}$	67	13	2
$R_{+0.05,\ P}$	7	22	2
$R_{+0.075,\ P}$	12	40	2
$R_{+0.1,\ P}$	14	70	3

Table 3: Time-to-alarm (seconds) for three second order step anomalies (high elevation case)

One problem observed during the initial collection of nominal data was that the mean value of some particular metrics did not remain constant across successive runs. For the Δ tests, these differences were negligible. For the other metrics, however, the difference between the means was actually larger than the span of the detection threshold, which would have resulted in a persistent alarm under operational conditions and rendered the detection algorithm substantially useless. This problem was rectified by replacing some of the RF cables in the experimental setup with semi-rigid lines, shielding the AWG channel switch, and repeating the calibration procedure.

CONCLUSIONS AND FUTURE WORK

This paper describes a prototype real-time signal quality monitor for GPS signals. The system is based on a pair of modified GPS receivers whose tracking channels are outfitted with supplementary correlators for the purpose of providing additional information about the correlation peaks being tracked. This information is then used to compute test metrics for each incoming signal in real time. The receivers can track both live and simulated GPS data.

An arbitrary GPS signal generator is also introduced. This apparatus is used to generate synthetic GPS signals, both nominal and distorted, which are tracked normally by the receivers in the RTSQM. The test metrics associated with these signals are recorded and analyzed.

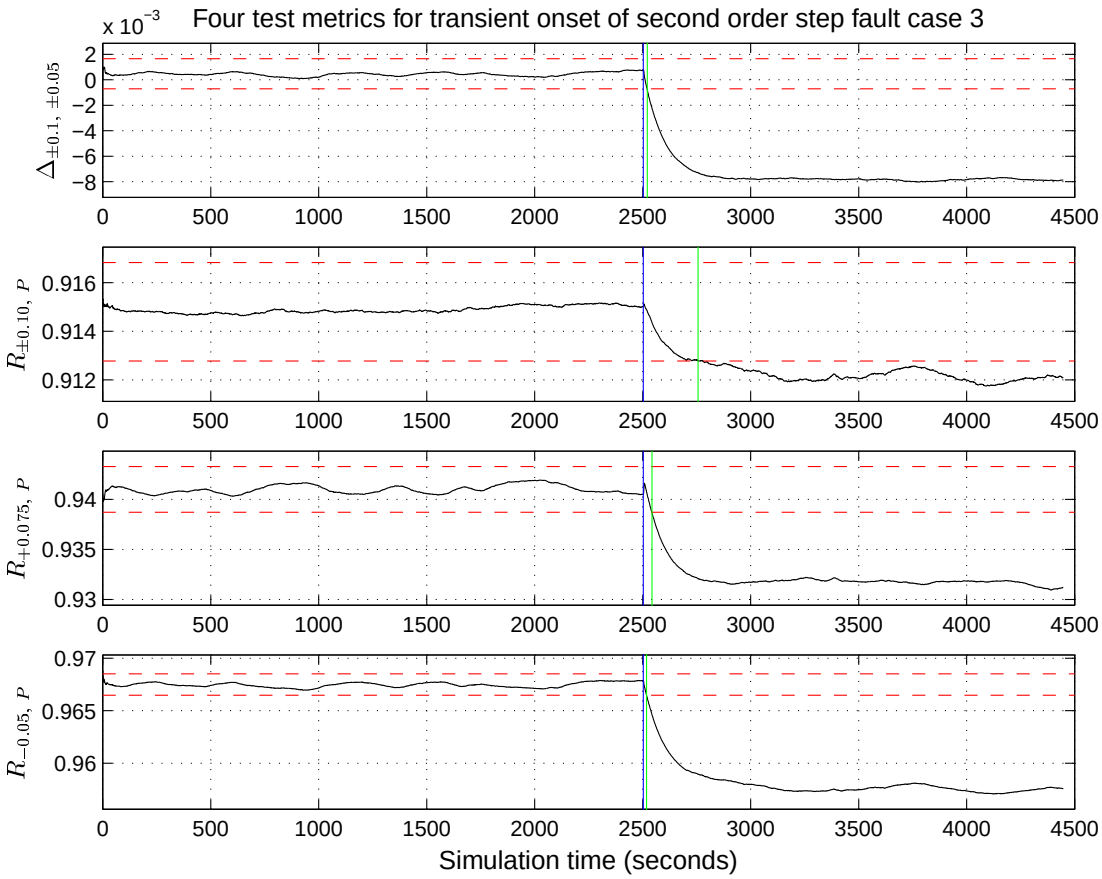

Figure 10: Test metrics for fault case 3

A class of signal failures known as the second order step anomaly is introduced and characterized. Several versions of this signal anomaly are programmed into the signal generator and the dynamic effects of these signals on the RTSQM are presented.

This research suggests several additional interesting experiments. First, the RF circuitry should be properly shielded and packaged, as noted in the previous section. A mixer with a higher output range might also improve the trackability of the synthetically generated signal at low carrier-to-noise ratios.

Second, it would be informative to repeat the dynamic signal fault tests several times to more precisely determine which test metrics are optimal for a given fault case.

A third set of questions worth investigating concerns overall system noise. The setup described in this research is entirely free of multipath distortion, whereas the experimentally determined thresholds in [5] were computed using live GPS data collected in a fairly harsh multipath environment. It should be possible to simulate the effects of multipath with careful programming of the AWG, additional RF hardware (splitters and long cables), or both.

Finally, the flexibility of the signal generator has not yet been fully exploited. For example, it would be interesting to compare the "instant-on" signal failures described in this paper with more subtle anomalies by varying the duty cycle between nominal and distorted waveforms within the AWG. Other simulations of interest would include additional second order step cases, as well as other signal fault models.

ACKNOWLEDGMENTS

The authors would like to thank the Federal Aviation Administration for their generous support of this research. Thanks also to all the members of the Stanford University GPS Lab for their insightful comments and suggestions.

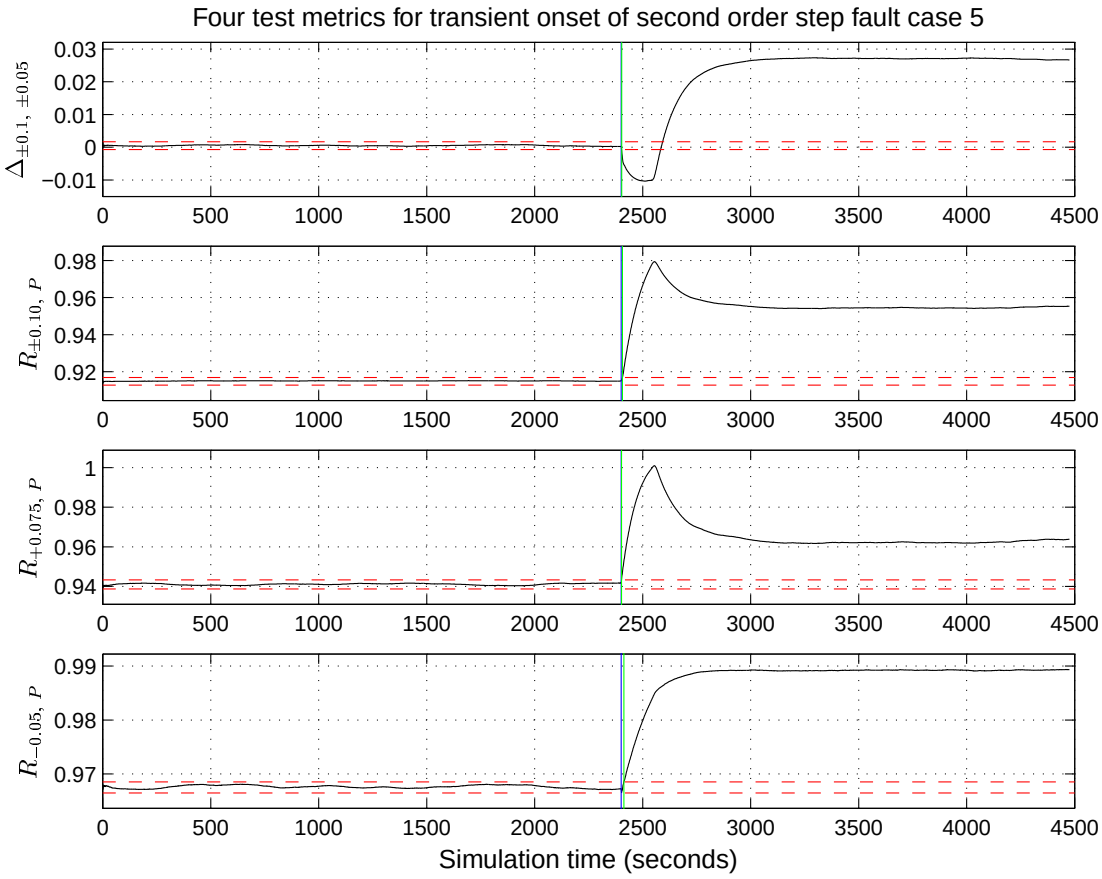

Figure 11: Test metrics for fault case 5

Test metric	Nominal Low	Nominal Mid	Nominal High	Fault case 1 Low	Fault case 1 Mid	Fault case 1 High	Fault case 3 High	Fault case 5 High
$\Delta_{\pm 0.075,\ \pm 0.05}$	-3.254e-3	8.459e-5	3.099e-4	-2.577e-3	-2.623e-3	-2.652e-3	-8.821e-4	1.131e-2
$\Delta_{\pm 0.1,\ \pm 0.05}$	-5.743e-3	1.119e-4	4.742e-4	-6.410e-3	-6.516e-3	-6.617e-3	-7.821e-3	2.704e-2
$R_{\pm 0.05,\ P}$	0.9580	0.9658	0.9675	0.9707	0.9701	0.9705	0.9577	0.9889
$R_{\pm 0.075,\ P}$	0.9274	0.9387	0.9413	0.9477	0.9469	0.9474	0.9307	0.9741
$R_{\pm 0.1,\ P}$	0.9002	0.9123	0.9148	0.9247	0.9240	0.9245	0.9121	0.9548
$R_{-0.05,\ P}$	0.9577	0.9657	0.9675	0.9707	0.9700	0.9706	0.9576	0.9892
$R_{-0.075,\ P}$	0.9238	0.9387	0.9416	0.9451	0.9442	0.9449	0.9296	0.9857
$R_{-0.1,\ P}$	0.8942	0.9123	0.9153	0.9184	0.9174	0.9179	0.9042	0.9819
$R_{+0.05,\ P}$	0.9583	0.9658	0.9676	0.9707	0.9702	0.9705	0.9579	0.9887
$R_{+0.075,\ P}$	0.9309	0.9387	0.9410	0.9502	0.9495	0.9500	0.9318	0.9625
$R_{+0.1,\ P}$	0.9062	0.9122	0.9144	0.9311	0.9305	0.9310	0.9201	0.9272

Table 2: Summary of expected values of test metrics

Test metric	FC 1 High	FC 1 Mid	FC 1 Low
$\Delta_{\pm 0.075,\ \pm 0.05}$	9	33	*n.d.*
$\Delta_{\pm 0.1,\ \pm 0.05}$	15	35	*n.d.*
$R_{\pm 0.05,\ P}$	33	50	33
$R_{\pm 0.075,\ P}$	28	43	35
$R_{\pm 0.1,\ P}$	22	36	38
$R_{-0.05,\ P}$	47	63	36
$R_{-0.075,\ P}$	61	63	25
$R_{-0.1,\ P}$	67	63	19
$R_{+0.05,\ P}$	7	38	32
$R_{+0.075,\ P}$	12	34	53
$R_{+0.1,\ P}$	14	32	73

Table 4: Time-to-alarm (seconds) for second order step anomaly fault case 1 (high, medium, and low elevation case)

References

[1] D. Akos, R. E. Phelts, A. Mitelman, S. Pullen, and P. Enge, "GPS-SPS Signal Quality Monitoring (SQM)," *Proc. IEEE-PLANS 2000,* San Diego, California, Mar. 2000.

[2] *Specification: Performance Type One Local Area Augmentation System Ground Facility.* U.S. Federal Aviation Administration Doc. No. FAA-E-2937, Washington, D.C., Sept. 1999.

[3] P. Enge, "Local area augmentation of GPS for the precision approach of aircraft," *Proc. IEEE,* vol. 87, pp. 111-132, Jan. 1999.

[4] A. J. Van Dierendonck, D. Akos, S. Pullen, R. E. Phelts, and P. Enge, "Practical Implementation Considerations in the Detection of GPS Satellite Signal Failure," *Proc. IAIN World Congress / ION Annual Meeting,* San Diego, California, June 2000.

[5] R. E. Phelts, D. Akos, and P. Enge, "SQM Validation Report for GNSSP WG-B Meeting," Department of Aeronautics and Astronautics, Stanford University, May 2000.

[6] P. Daly, S. Riley, and P. Raby, "Recent advances in the implementation of GNSS," *Proc. ION GPS-93,* Salt Lake City, Utah, Sept. 1993.

[7] H. S. Cobb *et. al.,* "Observed GPS signal continuity interruptions," *Proc. ION GPS-95,* Palm Springs, California, Sept. 1995.

[8] A. Hansen, T. Walter, P. Enge, and D. Lawrence, "GPS satellite clock event on SVN 27 and its impact on augmented navigation systems," *Proc. ION GPS-98,* Nashville, Tennessee, Sept. 1998.

[9] B. Parkinson and J. Spilker, Jr., eds. *Global Positioning System: Theory and Applications I,* Progress in Astronautics and Aeronautics, vol. 163, pp. 129-132, AIAA, Washington, D.C., 1996.